Transactions of the Materials Research Society of Japan 31[1] 65-68 (2006)

Ferroelectricity and Electronic State of $Bi_4Ti_{3-x}Hf_xO_{12}$ Ceramics

Tohru Higuchi, Shigetaka Watanabe, Yuki Ohno, Kyohei Natsume,
Takeshi Hattori and Takeyo Tsukamoto
Department of Applied Physics, Tokyo University of Science, 1-3 Kagurazaka, Shinjuku, Tokyo 162-8601, Japan
Fax: 81-3-5228-8241, e-mail: higuchi@rs.kagu.tus.ac.jp

The structural and ferroelectric properties of Hf-substituted $Bi_4Ti_3O_{12}$ ($Bi_4Ti_{3-x}Hf_xO_{12}$) dense bulk ceramics were investigated, and their electronic structures were measured by X-ray absorption spectroscopy (XAS) and soft-X-ray emission spectroscopy. The $Bi_4Ti_{3-x}Hf_xO_{12}$ dense bulk ceramics exhibit single phase and in the Hf concentration region of x=0~0.030. The lattice constant, which is expected from the crystal-filed splitting of Ti 2*p* XAS spectra, increases with increasing Hf^{4+} concentration. The remannet polarization of $Bi_4Ti_{3-x}Hf_xO_{12}$ is larger than that of undoped $B_4Ti_3O_{12}$. The valence band of $Bi_4Ti_{3-x}Hf_xO_{12}$ is mainly composed of the O 2*p* states hybridized with Ti 3*d* and Bi 6*s* states. The Ti-O hybridization effect does not depend on Hf^{4+} concentration. The Bi-O hybridization effect depends on Hf^{4+} concentration. These findings indicate that the Bi^{3+} with lone pair 6*s* electron is closely related with the ferroelectricity of $Bi_4Ti_3O_{12}$.

Key words: $Bi_4Ti_{3-x}Hf_xO_{12}$, ceramics, ferroelectricity, electronic structure, hybridization effect

1. INTRODUCTION

Ferroelectric thin films have attracted considerable attention because of their use in ferroelectric random access memories (FeRAMs). Most of the attention has been focused on bismuth layer-structured ferroelectrics, such as $Bi_4Ti_3O_{12}$ (BIT) and $SrBi_2Ta_2O_9$ [1-3]. In particular, the BIT exhibits a spontaneous polarization in the *a-c* plane at an angle of about 4.5 ° to the *a*-axis, and exhibits two independently reversible components along the *c*- and *a*-axes. The *c*-axis oriented BIT thin films are expected to be applied to nonvolatile FeRAM device with nondestructive readout operation because of their low dielectric constant and small coercive field. Furthermore, the BIT thin films are considered promising due to their excellent fatigue endurance when used with a Pt electrode.

In recent years, La-doped BIT ($Bi_{4-x}La_xTi_3O_{12}$) has been reported as a promising material to solve poor fatigue of BIT. The $Bi_{4-x}La_xTi_3O_{12}$ thin film, which was prepared at a low temperature of 650°C, exhibits a relatively large remanent polarization, and superior fatigue endurance was confirmed [4-6]. Such a significant improvement in ferrolectricity has been observed only for $(Bi_{4-x}La_x)(Ti_{3-y}V_y)O_{12}$ and $Bi_4Ti_{3-y}V_yO_{12}$ films. This selective control of each site is named "site-engineering". The effect of the site-engineering technique for BIT has been extensively studied by Watanabe and co-workers [7-10]. They reported that the major contribution of site-engineering for BIT is to adjust the Curie temperature and to suppress the domain pinning. Therefore, understanding structural properties of selective controlled BIT is one of the most important subjects in term of FeRAM applications.

In this study, we have prepared Hf-doped BIT ($Bi_4Ti_{3-x}Hf_xO_{12}$) ceramics and studied its electronic state. The structural properties were characterized by soft-X-ray emission spectroscopy (SXES) and X-ray absorption spectroscopy (XAS). It is generally known that photoemission spectroscopy (PES) is a powerful technique for the investigation of the electronic structure. The PES is surface sensitive and charging for insulator. Thus, it is difficult to study the electronic structure of a ferroelectric material by PES. SXES and XAS can confirm the electronic structure in the bulk state, because the mean free path of a soft-X-ray is very long compared with that of an electron. On the other hand, the SXES spectra, which have clear selection rules regarding the angular momentum due to dipole transition, reflect the occupied partial density-of-state (DOS). The XAS is related directly to the unoccupied DOS. This optical process is rather local process, because of the localized core state. It is governed by dipole selection rules so that XAS gives the spectrum related to the site- and symmetry-selected DOS.

2. EXPERIMENTAL

$Bi_4Ti_{3-x}Hf_xO_{12}$ ceramics were prepared by conventional solid state reaction method. The Bi_2O_3, TiO_2 and HfO_2 powders with purity of 99.99 % were mixed. The mixed powder calcinated at 800°C for 7 h was crushed and then pressed into pellets. These pellets were sintered at 1200°C for 4 h. The relative density of $Bi_4Ti_{3-x}Hf_xO_{12}$ ceramic was approximately 98 %. The Hf concentrations were x=0~0.03. The structural properties of these ceramics were characterized by X-ray diffraction (XRD) using CuKα. The polarization-electric field (*P-E*) hysteresis loops were measured using a conventional Sawyer-Tower circuit with a sinusoidal field.

XAS and SXES measurements were carried out at the revolver undulator beamline BL-19B at the Photon Factory of the High Energy Accelerator Organization, in

Tsukuba, Japan. High brightness and high resolution were realized using a varied-line-spacing plane grating monochrometer. The XAS spectra were measured by a Si photodiode. The SXES spectra were measured by a soft-X-ray emission spectrometer. The spectrometer used the Rowland circle geometry that consisted of a grating with a groove density of 300 lines/mm and a Cs-coated multichannel detector. The total resolutions of XAS and SXES were approximately 0.1 eV and 0.4 eV, respectively, at $h\nu$=450 eV.

3. RESULTS AND DISCUSSION

Figure 1 shows the XRD patterns as a function of Hf concentration in $Bi_4Ti_{3-x}Hf_xO_{12}$ ceramics. These XRD patterns exhibit the single phase. The apparent change of the lattice parameter is not observed in this substitution region. Similar result has been reported in Zr-substituted $Bi_4Ti_3O_{12}$ ($Bi_4Ti_{3-x}Zr_xO_{12}$). For Nd-substituted $Bi_4Ti_3O_{12}$ ($Bi_{4-x}Nd_xTi_3O_{12}$), the lattice constants of *a*- and *b*-axes decrease from 5.45 Å to 5.40 Å and from 5.41 Å to 5.40 Å, respectively, at $0 < x < 1.5$ [11]. This contributes to the differences of substitution site and concentration. The detailed results of structural analysis for $Bi_4Ti_{3-x}Hf_xO_{12}$ ceramics well be published elsewhere.

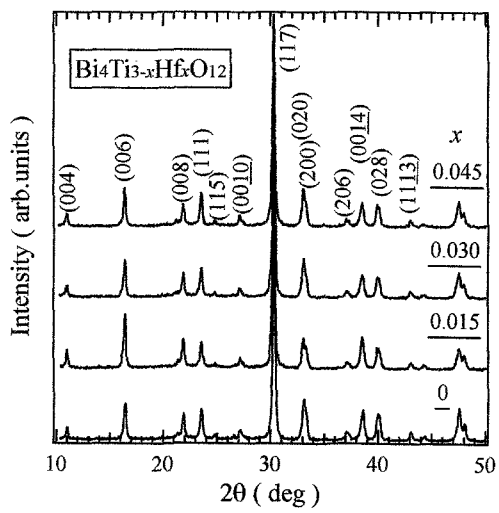

Fig. 1 XRD patterns as a function of Hf concentration in $Bi_4Ti_{3-x}Hf_xO_{12}$ ceramics.

Figure 2 shows the Ti 2*p* XAS spectra as a function of Zr^{4+} concentration in $Bi_4Ti_{3-x}Hf_xO_{12}$ ceramics. The Ti 2*p* XAS spectra correspond to the transition from Ti 2*p* core level to unoccupied Ti 3*d* state. The spectra are derived from the two parts of L_3 ($2p_{3/2}$) and L_2 ($2p_{1/2}$). They are split into the t_{2g}- and e_g-subbands by the octahedral ligand field [12]. The intensity of t_{2g}-subband decreases with increasing Hf^{4+} concentration. This result indicates that the doped Hf^{4+} ions enter the Ti^{4+} site of BIT. The energy separation between t_{2g}- and e_g-subbands corresponds to the crystal-field splitting (10Dq). According to the ligand-field theory, the magnitude of 10Dq is determined by ion radius, electron

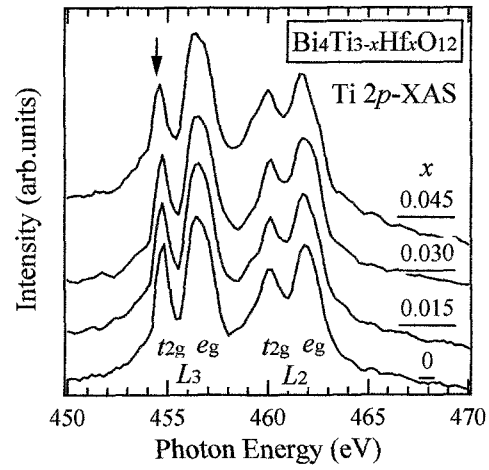

Fig. 2 Ti 2*p* XAS spectra as a function of Hf^{4+} concentration in $Bi_4Ti_{3-x}Hf_xO_{12}$ ceramics.

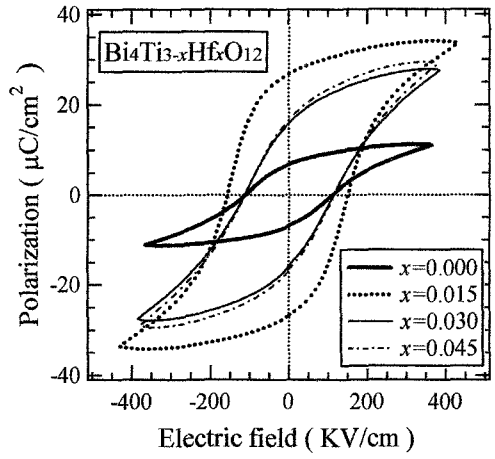

Fig. 3 *P-E* hysteresis loops as a function of Hf cocentration in $Bi_4Ti_{3-x}Hf_xO_{12}$ ceramics.

mass, element number, and lattice constant. The 10Dq does not depend on the Nd^{3+} concentration. This result accords with the XRD patterns of Fig. 1.

Figure 3 shows the *P-E* hysteresis loops as a function of Hf concentration in $Bi_4Ti_{3-x}Hf_xO_{12}$ ceramics. The *P-E* hysteresis loops are observed in all Hf concentrations. In particular, the sample of x=0.015 is characterized by a well-saturated *P-E* hysteresis loop. The P_r of x=0.015, 0.030, and 0.045 were $2P_r$ =52.4 μC/cm^2, 31.2 μC/cm^2 and 32.5 μC/cm^2, respectively. These values of $Bi_4Ti_{3-x}Hf_xO_{12}$ ceramics are larger than those of stoichiometric $Bi_4Ti_3O_{12}$ ceramics. The E_c of x=0.015, 0.030, and 0.045 were $2E_c$=304 kV/cm, 226 kV/cm and 225 kV/cm, respectively. The small E_c and large P_r are considered to be due to effect of Hf substitution into Ti site.

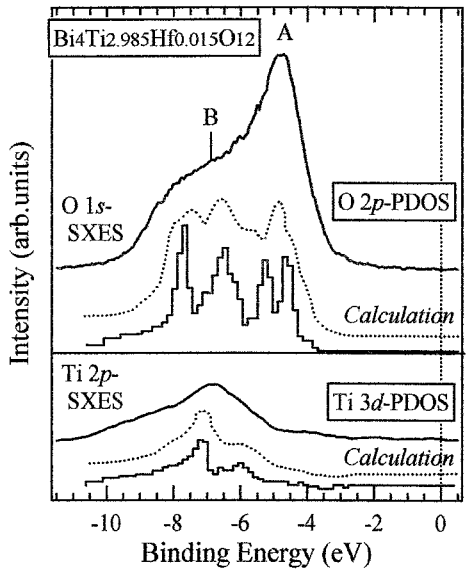

Fig. 4: O 1*s* and Ti 2*p* SXES spectra of $Bi_4Ti_{2.985}Hf_{0.015}O_{12}$ ceramics. For reference, the calculated band DOS is also shown under each SXES spectrum.

Figure 4 shows the O 1*s* and Ti 2*p* SXES spectra in the valence band region of $Bi_4Ti_{2.985}Hf_{0.015}O_{12}$ ceramics. The O 1*s* SXES spectrum measured at hv=500 eV reflects the O 2*p* partial-DOS (PDOS). The Ti 2p SXES spectrum measured at *hv*=550 eV reflects the Ti 3*d* PDOS. One can find that the energy position of the O 2*p* state overlaps with that of the Ti 3*d* state in the valence band. The valence band has two peaks, A and B, at -5.2 eV and -7.5 eV, respectively. Comparing both SXES spectra the Ti 3*d* contribution is more significant on the higher energy side (peak B), where the O 2*p* states have a larger admixture of the Ti 3*d* state. On the other hand, the valence band derived from the O 2*p* states are hybridizes with the Ti 3*d* states. Therefore, we can conclude that peak A corresponds to the nonbonding state and peak B corresponds to the bonding state that is well mixed with the Ti 3*d* state [13-17].

In Fig. 4, the PDOS histogram calculated in undoped BIT is also shown under each SXES spectrum. The electronic structure calculations based on the density functional theory using local density approximation (LDA) were performed using the *ab-initio* calculation program. In order to calculate the electronic structure, we optimized the bases sets with effective core potential. A dashed curve above each calculated PDOS histogram is obtained by convoluting the original PDOS with Gaussian broadening functions with a width of 0.5 eV, which reflects the total resolution of the experimental system. The calculated O 2*p* PDOS has four peaks, which correspond to G, X, P, and N points in the tetragonal Brilliouin zone [15,16]. Although the O 1*s* SXES spectrum has only two peaks, this is considered to be due to the poor resolution of the experimental system. However, the bandwidths of the calculated PDOS are in good agreement with those of the Ti 2*p* and O 1*s* SXES spectra.

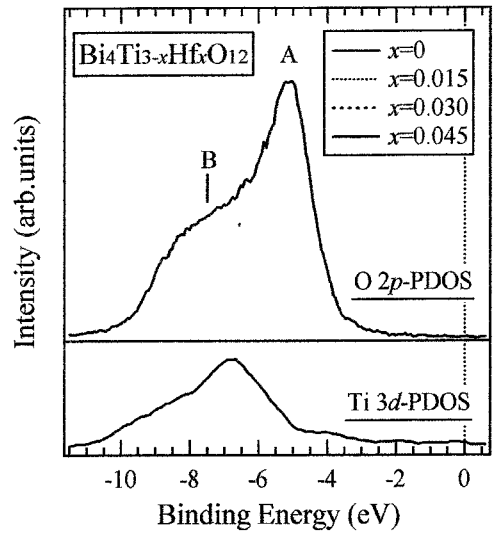

Fig. 5: O 1*s* and Ti 2*p* SXES spectra as functions of Hf concentration in $Bi4Ti_{3-x}Hf_xO_{12}$ ceramics.

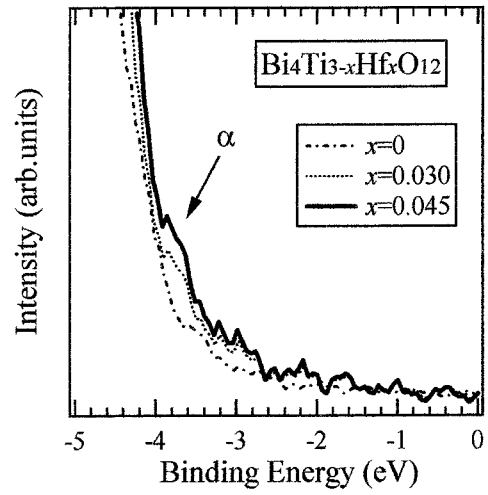

Fig. 6 O 2*p* PDOS at the top of the valence band as a function of Hf concentration in $Bi_4Ti_{3-x}Hf_xO_{12}$ ceramics. The peak α, which corresponds to the top of the valence band of Fig. 5, is the O 2*p* state hybridized with Bi 6*s* state.

Figure 5 shows O 1*s* and Ti 2*p* SXES spectra as functions of Hf concentration in $Bi_4Ti_{3-x}Hf_xO_{12}$ ceramics. The intensities of the SXES spectra are normalized by the intensity of the elastic scattering, although the elastic scattering peak is not shown in this figure. At all dopant concentrations, it is clear that the O 2*p* state hybridizes with the Ti 3*d* state in the valence band, as shown in the case of the $Bi_4Ti_{3-x}Hf_xO_{12}$ ceramics in Fig. 4. The bandwidth and Ti-O hybridization effect of $Bi_4Ti_{3-x}Hf_xO_{12}$ ceramics does not depend on Hf concentration. In $Bi_{4-x}Nd_xTi_3O_{12}$, the Ti-O hybridization effect increases with increasing Nd concentration. This corresponds to the decrease of Ti-O bond length with the lattice constant. However, the apparent change of lattice constant is not observed in

Fig. 1. Thus, the Ti-O hybridization effect does not depend on $Bi_4Ti_{3-x}Hf_xO_{12}$ ceramics.

Figure 6 shows the detailed O 1*s* SXES spectra at the top region of the valence band as a function of Hf^{4+} concentration in $Bi_4Ti_{3-x}Hf_xO_{12}$ ceramics. The peak α of the spectrum corresponds to that of Fig. 5. The top of the valence band is the O 2*p* state hybridized with Bi 6*s* state, which has reported in the band calculation of ref.16. Comparing the detailed O 1*s* SXES spectra, the intensity of peak α decreases with increasing Hf^{4+} concentration. This finding indicates that the hybridization effect between Bi 6*s* state and O 2*p* state increases with Hf^{4+} concentration.

The above result indicates that the Bi 6*s* orbital is fully occupied and acts as a lone pair state. This behavior is similar to the Pb 6*s* orbital in $PbTiO_3$ [18, 19]. In $SrBi_2Ta_2O_9$, the Bi state is asymmetric and the Bi lone pair lies off center and points out of the Bi_2O_2 layer, in a fashion similar to the Pb 6*s* lone pair in PbO. The ferroelectric behavior is amplified by the off-center displacements of the Bi and $SrBi_2Ta_2O_9$ and Pb in $PbTiO_3$. Such an effect is also expected in $Bi_4Ti_{3-x}Hf_xO_{12}$. The displacements of these ions are considered to be driven by the lone pair *s* electrons, though the detailed origin has not been clarified in this study.

4. CONCLUSION

We prepared the $Bi_4Ti_{3-x}Hf_xO_{12}$ ceramics and studied their structural and ferroelectric properties. The prepared ceramics exhibited the $Bi_4Ti_{3-x}Hf_xO_{12}$ single phase. The intensity of Ti 2*p* XAS spectra of $Bi_4Ti_{3-x}Hf_xO_{12}$ ceramics decreases with increasing Hf concentration, indicating that the doped Hf ions enter the Ti^{4+} site. The remannet polarization of $Bi_4Ti_{3-x}Hf_xO_{12}$ is larger than that of undoped $B_4Ti_3O_{12}$. The valence band of $Bi_4Ti_{3-x}Hf_xO_{12}$ is mainly composed of the O 2p states hybridized with Ti 3*d* and Bi 6*s* states. The Ti-O hybridization effect does not depend on Hf^{4+} concentration. The Bi-O hybridization effect depends on Hf^{4+} concentration. These findings indicate that the Bi^{3+} with lone pair 6*s* electron is closely related with the ferroelectricity of $Bi_4Ti_3O_{12}$.

ACKNOWLEDGEMENT

We would like to thank Prof. S. Shin for his useful discussion. This work was supported by a Grant-In-Aid for Scientific Research from the Ministry of Education, Culture, Sports, Science and Technology.

REFERENCES

[1] E. C. Subbarao: Phys. Rev. **122** (1961) 804.
[2] S. E. Cummins and L. E. Cross: Appl. Phys. Lett. **10** (1967) 14.
[3] R. W. Wolfe and R. E. Newnham: J. Electrochem. Soc. **116** (1967) 832.
[4] B. H. Park, B. S. Kang, S. D. Bu, T. W. Noh, J. Lee and W. Jo: Nature **410** (1999) 682.
[5] U. Chon, G. Yi and H. M. Jang, Appl. Phys. Lett. **78** (2001) 658.
[6] Y. Hou, X. Xu, H. Wang, M. Wang and S. Shang, Appl. Phys. Lett. **78** (2001) 1733.
[7] T. Watanabe, A. Saiki, K. Saito and H. Funakubo: J. Appl. Phys. **89** (2001) 3934.
[8] E. Tokumitsu, T. Isobe, T. Kijima and H. Ishiwara: Jpn. J. Appl. Phys. **40** (2001) 5576.
[9] T. Watanabe, T. Kojima, T. Sakai, H. Funakubo, M. Osada, Y. Noguchi and M. Miyayama: J. Appl. Phys. **92** (2002) 1518.
[10] T. Watanabe, H. Funakubo, M. Osada, Y. Noguchi and M. Miyayama: Appl. Phys. Lett. **80** (2002) 100.
[11] T. Goto, Y. Noguchi, M. Soga and M. Miyayama: Mater. Res. Bull. **40** (2005) 1044.
[12] T. Higuchi, T. Tsukamoto, M. Watanabe, M. M. Grush, T. A. Callcott, R. C. Perera, D. L. Ederer, Y. Tokura, Y. Harada, Y. Tezuka and S. Shin, Phys. Rev. B **60** (1999) 7711.
[13] T. Higuchi, T. Tsukamoto, K. Kobayashi, S. Yamaguchi, Y. Ishiwata, N. Sata, K. Hiramoto, M. Ishigame and S. Shin: Phys. Rev. B **65** (2002) 33201.
[14] T. Higuchi, M. Tanaka, K. Kudoh, T. Takeuchi, Y. Harada, S. Shin and T. Tsukamoto: Jpn. J. Appl. Phys. **40** (2001) 5803.
[15] T. Higuchi, K. Kudoh, T. Takeuchi, Y. Masuda, Y. Harada, S. Shin and T. Tsukamoto: Jpn. J. Appl. Phys. **41** (2002) 7195.
[16] T. Higuchi, Y. Moriuchi, M. Satake, T. Hattori and T. Tsukamoto: Trans. Mater. Res. Soc. Jpn. **30** (2005) 15.
[17] T. Higuchi, T. Goto, Y. Noguchi, M. Miyayama, T. Hattori and T. Tsukamoto: Trans. Mater. Res. Soc. Jpn. **30** (2005) 11.
[18] R. E. Cohen: Nature **358** (1992) 136.
[19] R. E. Cohen and H. Krakauer: Phys. Rev. B **42** (1990) 6416.

(Received December 10, 2005; Accepted January 31, 2006)